

Timescale for equilibration of N/Z gradients in dinuclear systems

K. Brown,¹ S. Hudan,^{1,*} R. T. de Souza,^{1,†} J. Gauthier,² R. Roy,² D. V. Shetty,³ G. A. Souliotis,^{3,4} and S. J. Yennello³

¹ *Department of Chemistry and Center for Exploration of Energy and Matter
2401 Milo B. Sampson Lane, Bloomington IN 47405, USA*

² *Université Laval, Québec, Canada*

³ *Cyclotron Institute, Texas A&M University, College Station, TX 77843, USA*

⁴ *Laboratory of Physical Chemistry, Department of Chemistry,
National and Kapodistrian University of Athens, Athens 15771, Greece*

(Dated: January 12, 2013)

Equilibration of N/Z in binary breakup of an excited and transiently deformed projectile-like fragment (PLF*), produced in peripheral collisions of $^{64}\text{Zn} + ^{27}\text{Al}$, ^{64}Zn , ^{209}Bi at $E/A = 45$ MeV, is examined. The composition of emitted light fragments ($3 \leq Z \leq 6$) changes with the decay angle of the PLF*. The most neutron-rich fragments observed are associated with a small rotation angle. A clear target dependence is observed with the largest initial N/Z correlated with the heavy, neutron-rich target. Using the rotation angle as a clock, we deduce that N/Z equilibration persists for times as long as 3-4 zs ($1\text{zs} = 1 \times 10^{-21}\text{s} = 300 \text{ fm/c}$). The rate of N/Z equilibration is found to depend on the initial neutron gradient within the PLF*.

PACS numbers: 25.70.Mn, 25.70.Lm

The broad impact of the density dependence of the nuclear symmetry energy makes it a topic of considerable interest. Whether the asymmetry term in the nuclear equation of state follows a stiff or a soft dependence on density determines the composition of a neutron star's crust, and the conditions under which a supernova explosion occurs [1–3]. In the case of nuclei, the stability of the heaviest elements [4], and the existence of neutron skins [5], also depend on this quantity. One means of investigating the density dependence of the symmetry energy is by measuring the N/Z equilibration in a dinuclear system [6–8]. Although past studies have principally focused on the N/Z equilibration that occurs between the projectile and target nuclei in a collision, such an approach is fundamentally limited by the short contact time between the two collision partners. This contact time, which is approximately 100 fm/c at intermediate energies, inherently limits the degree of equilibration that can be attained.

Another opportunity to investigate N/Z equilibration is the dynamical binary breakup of an excited and transiently deformed nucleus produced in the semi-peripheral collision of two heavy-ions at intermediate energies ($E/A=20\text{-}100$ MeV) [9]. At these energies, the collision of two heavy-ions at peripheral and mid-central impact parameters leads to the exchange of charge, mass, and energy between the projectile and target nuclei and results in the production of two nuclei designated the projectile-like (PLF*) and target-like (TLF*) nuclei. Following their separation, these two nuclei that are excited and transiently deformed, subsequently decay. In the

first application of this approach it was recently determined that N/Z equilibration persists for timescales as long as $t \approx 3\text{zs}$ ($1\text{zs} = 1 \times 10^{-21}\text{s}$) [10].

In the present work we further characterize this approach, expanding it to a significantly lighter projectile. We explore the impact of the N/Z of the target on the composition of the fragments produced and their subsequent evolution. We also demonstrate that this equilibration process exists when the projectile and target nuclei are the same.

The experiment was conducted at the Cyclotron Institute at Texas A&M University, where a beam of ^{64}Zn ions was accelerated to $E/A = 45$ MeV with an average beam intensity of $\approx 2 \times 10^8$ p/s. The beam impinged on ^{27}Al , ^{64}Zn and ^{209}Bi targets with thicknesses of 13.4, 5, and 1 mg/cm² respectively. Although the experimental details have been previously published [11], they are summarized below for completeness. The array FIRST [12], which subtended the angular range $4.5^\circ \leq \theta_{lab} \leq 27^\circ$ was used to identify charged products produced in the reaction. In the angular range $4.5^\circ \leq \theta_{lab} \leq 7^\circ$, the forward telescope in FIRST provided identification by atomic number of all products up to $Z=30$ and isotopic information for $Z \leq 12$. The second telescope in FIRST, which subtended the angular range $7^\circ \leq \theta_{lab} \leq 14^\circ$, provided Z identification for $Z \leq 22$ and A identification for $Z \leq 8$. The third telescope in FIRST ($14^\circ \leq \theta_{lab} \leq 27^\circ$) provided Z identification for $Z \leq 12$ and A identification for $Z \leq 7$. The high segmentation of FIRST provided an angular resolution of $\pm 0.05^\circ$ ($4.5^\circ \leq \theta_{lab} \leq 7^\circ$), $\pm 0.44^\circ$ ($7^\circ \leq \theta_{lab} \leq 14^\circ$) and $\pm 0.81^\circ$ ($14^\circ \leq \theta_{lab} \leq 27^\circ$) in polar angle and $\pm 11.25^\circ$ in azimuthal angle. The energy resolution obtained was approximately 1%.

In order to focus on binary decays, events were selected in which two fragments ($Z \geq 3$) were detected within the laboratory angular range $4.5^\circ \leq \theta_{lab} \leq 27^\circ$. These two

*Electronic address: shudan@indiana.edu

†Electronic address: desouza@indiana.edu

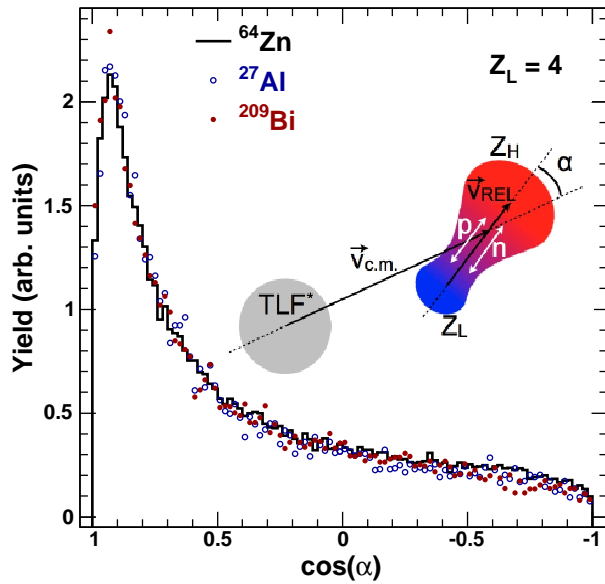


FIG. 1: (Color online) The angular distribution of binary splits (Z_L - Z_H) for $Z_L=4$, representative of other fragments, is shown. Data for the ^{64}Zn , ^{27}Al , and ^{209}Bi targets are represented by the black line, blue open symbol and red closed symbol histograms respectively.

fragments were distinguished from each other by their atomic number, with the larger (smaller) atomic fragment designated as Z_H (Z_L). We ensured that the PLF* under investigation comprised a large fraction of the initial projectile by requiring that the events selected had $Z_H > 11$. Events selected in this manner corresponded to approximately 14% of the measured yield in which one fragment with $Z > 11$ was detected.

It has previously been established that an instructive quantity for the binary decay of the PLF* is the angle between the direction of the two fragments center-of-mass velocity, $v_{c.m.}$ and their relative velocity, v_{REL} [13, 14]. We construct this angle α , as indicated within the inset of Fig. 1, with the relative velocity vector, v_{REL} , defined as $v_{REL} = v_H - v_L$. Consequently, aligned decays with Z_L emitted backward (forward) of Z_H corresponds to $\cos(\alpha) = 1$ (-1). Momentum correlations observed between Z_H and Z_L reveal that these two fragments originate from a common parent [14]. This parent nuclear system comprised of Z_H and Z_L is designated as the PLF*.

The angular distribution for $Z_L=4$ fragments is presented in Fig. 1 for the ^{64}Zn , ^{27}Al , and ^{209}Bi targets used. Consistent with previous work, all the angular distributions manifest a peak at backward angles $\cos(\alpha) > 0.5$. This preferential backward decay of the PLF* is well established, and has been interpreted as the aligned dynamical decay of the excited and transiently deformed PLF* [13, 15, 16]. The backward peaking of the angular distribution can be understood as the dynamical binary splitting of the PLF* on a timescale that is short relative to the rotational period of the PLF*. To compare the shape for the different targets, all three distributions

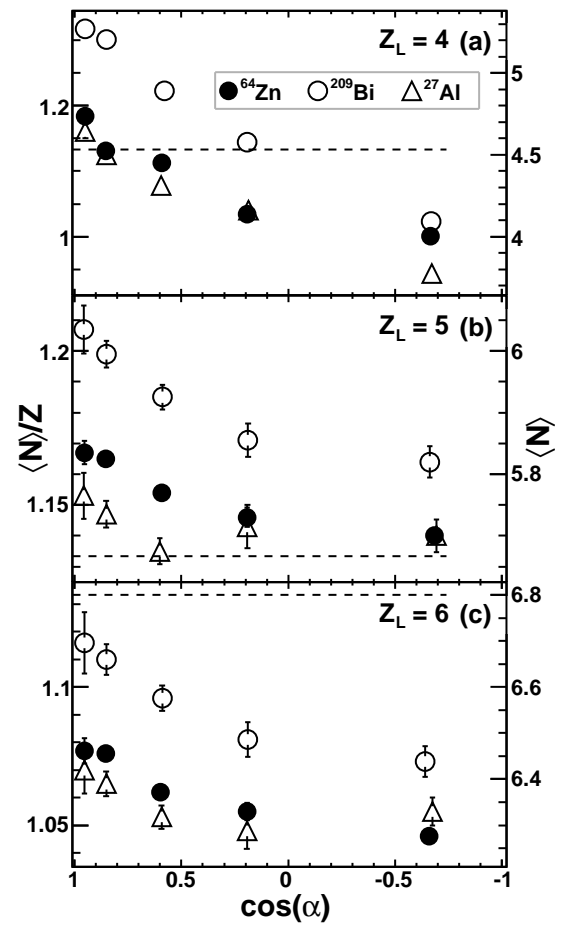


FIG. 2: Average neutron to proton ratio for selected Z_L as a function of the decay angle. The ratio for the ^{64}Zn , ^{209}Bi , and ^{27}Al targets is represented by the closed circle, open circle and open triangle respectively. The dashed line for each Z_L represents the N/Z of the ^{64}Zn beam.

have been normalized in the interval $-1 \leq \cos(\alpha) < 0$. We chose this region for normalization since it corresponds to forward statistical emission from the PLF*. This forward statistical decay is long-lived relative to backward emission and hence is less coupled to any dynamics responsible for the formation of the PLF*. For each target, the angular distributions exhibit the same shape, manifesting a distinct preference for aligned decay of the PLF* with the Z_L fragment oriented towards the target. The shape of the distribution for $\cos(\alpha) < 0$ provides an indication that the angular momentum of the decaying PLF* is relatively small. In contrast to previously studied systems [10], the yield does not increase near $\cos(\alpha) = -1$.

Given the normalization at forward angles, the similarity of the distributions for the three targets at backward angles, $\cos(\alpha) > 0$, is striking. This similarity suggests that while the probability of forming the elongated and excited PLF*, as well as its composition, may depend on the target, the relative probability of its subsequent decay is essentially independent of the target.

We next examine whether the composition of the Z_L

fragment changes as a function of rotation angle. In our initial work, which analyzed the reaction $^{124}\text{Xe} + ^{112,124}\text{Sn}$, we observed that the $\langle N \rangle / Z$ of the Z_L fragment decreased as the Z_L - Z_H system rotated [10]. As the Zn-like PLF* in the present work is considerably smaller than the Xe-like PLF*, it was unclear whether the behavior previously observed would also exist for the smaller PLF*. Depicted in Fig. 2 is the $\langle N \rangle / Z$ of the Z_L fragment for Be (a), B (b), and C (c) fragments. For each Z_L shown the impact of the three different targets is also presented. The average $\langle N \rangle / Z$ for a given Z_L is deduced by averaging the neutron number for the different isotopes measured. A common feature of all the data is that the largest value of $\langle N \rangle / Z$ is associated with $\cos(\alpha)=1$, namely backward emission. As the Z_L - Z_H system rotates, $\langle N \rangle / Z$ of the Z_L fragment decreases corresponding to a net loss of neutrons by the Z_L fragment. In the case of the Be fragments, this dependence of $\langle N \rangle / Z$ on $\cos(\alpha)$ is clearly apparent even for the lightest target, Al. For all three fragments shown the magnitude of $\langle N \rangle / Z$ is largest for the Bi target. We attribute this large value of $\langle N \rangle / Z$ for $\cos(\alpha) \approx 1$ in the case of the Bi target to the preferential pickup of neutrons by the PLF* from the Bi target with its $N/Z=1.51$. In contrast, the ^{64}Zn and ^{27}Al targets with $N/Z = 1.13$ and 1.07 do not present a neutron-rich reservoir from which the PLF* can pick up neutrons.

Shown in the right hand scale of Fig. 2 is the $\langle N \rangle$ of the Z_L fragment. In the case of the Be fragments, for the Bi target $\langle N \rangle$ decreases from 5.2 to 4.05 a net change of over one neutron. For the Zn and Al targets, a somewhat smaller net decrease of 0.6 - 0.7 in neutron number is observed. For the Bi target, the change in $\langle N \rangle$ for $Z_L=5$ and $Z_L=6$ is ≈ 0.2 . The change in $\langle N \rangle$ for Li fragments and the Bi target (not shown) is also ≈ 0.2 , comparable to that of B and C fragments. The larger change observed in the case of Be fragments can be qualitatively understood as being due to the absence of ^8Be fragments. Since the isotopic distribution for all the fragments with $Z_L=3,5$, and 6 has a value of $\langle N \rangle / Z > 1$, it is reasonable to expect that this is also the case for Be fragments. The decay of ^8Be into two alpha particles removes these fragments from the measured isotopic distribution thus artificially increases the value of $\langle N \rangle$ observed for Be at backward angles. In effect, the absence of ^8Be acts as an amplifier for the change in $\langle N \rangle$ by emphasizing the importance of the extremes of the isotopic distribution. For this reason, we have elected at present to present the ^8Be data without correcting for the absence of ^8Be .

The physical picture that emerges is one in which the N/Z of the dinuclear PLF* is established through its interaction with the target. Preferential transfer of neutrons from a neutron-rich target such as Bi results in a neutron-rich PLF*. As the nascent Z_L fragment is oriented towards the TLF, it is the primary beneficiary of the transferred neutrons. The result is an initial N/Z gradient within the PLF*. As time passes, these additional neutrons in the Z_L fragment are dissipated. Whether this

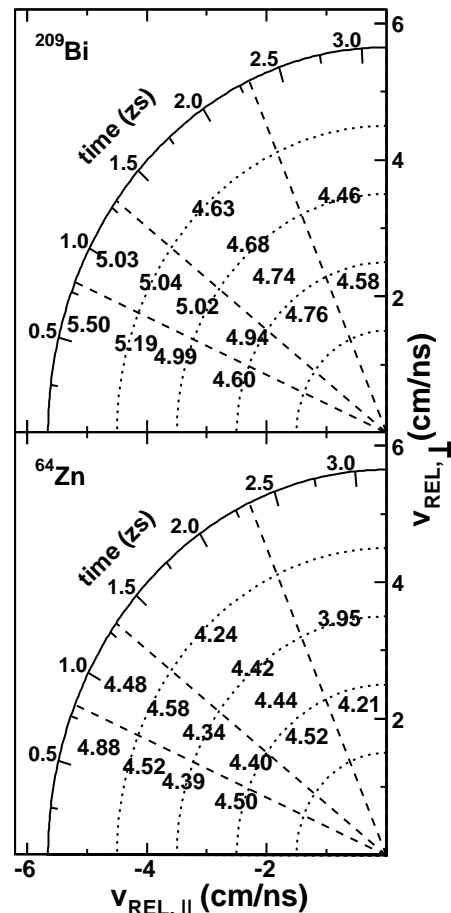


FIG. 3: Dependence of the average neutron number on the parallel and transverse components of v_{REL} for $Z_L = 4$ for the reactions $^{64}\text{Zn} + ^{209}\text{Bi}$, ^{64}Zn . (See text for details)

preferential neutron transport out of the Z_L fragment occurs into the Z_H fragment or into a low-density neck region connecting the Z_L and Z_H fragments is presently unclear [17]. It should be clear that transfer of both neutrons and protons occurs between the Z_H and Z_L fragments. Our selection of a particular Z_L fragment in this analysis precludes us from examining the net proton exchange.

If the decrease in $\langle N \rangle / Z$ with $\cos(\alpha)$ can be understood as the preferential transport of neutrons out of the Z_L fragment, one might expect that the shorter the contact time between the Z_L and Z_H fragments the less likely it is that the initial $\langle N \rangle / Z$ is decreased. Dynamical splitting of the dinuclear Z_H - Z_L system can be viewed as a dynamical fission process in which the reaction dynamics provides collective motion along the separation axis of the Z_L - Z_H system [13, 14, 18]. Within such a picture we expect that the shortest times (dynamical ruptures) are associated with the largest relative velocities and the longest times are associated with smallest (Coulomb barrier) relative velocities.

In order to explore the dependence of $\langle N \rangle / Z$ on both

$\cos(\alpha)$ and v_{REL} , we present the dependence of $\langle N \rangle$ of Be fragments in velocity space in Fig. 3. In this figure, the dependence of the average neutron number, $\langle N \rangle$, of Be fragments on the transverse ($v_{REL,\perp}$) and parallel ($v_{REL,\parallel}$) components of v_{REL} is depicted. The parallel and transverse components of v_{REL} are calculated with respect to the center-of-mass velocity of the Z_L - Z_H system. For reference, relative velocities between 1.5 and 5.5 cm/ns are indicated as dotted circles while the angular cuts over which the average neutron number was calculated are represented by dashed lines.

For the ^{209}Bi (top panel) target a systematic behavior of $\langle N \rangle$ of the Be fragment is observed. As one rotates clockwise in the two dimensional velocity space, i.e. increasing rotation angle α , the value of $\langle N \rangle$ decreases. For the largest v_{REL} , the $\langle N \rangle$ of the Z_L fragment decreases from 5.5 to 4.46, a change of ≈ 1 neutron as the Z_H - Z_L system rotates by a quarter turn. For the two most backward angle bins one observes that $\langle N \rangle$ decreases with decreasing $v_{REL,\parallel}$ (from 5.5 to 4.6), while for larger rotation angles, $\langle N \rangle$ increases with decreasing $v_{REL,\parallel}$ (from 4.46 to 4.58). From this trend, one would predict that $\langle N \rangle$ and hence $\langle N \rangle/Z$ would decrease with increasing v_{REL} for forward emission. This expectation is confirmed for this system in agreement with previous observation [10]. These trends are also observed for the ^{64}Zn (bottom panel) target although the magnitude is slightly smaller than in the ^{209}Bi case.

To extract the time dependence of the $\langle N \rangle$ of the Be fragment, we utilize the rotation angle of the Z_L - Z_H dinuclear system as a clock. The angular momentum of the dinuclear complex is determined by utilizing a simple model to describe the forward part of the angular distribution. This simple model has been successfully used to describe the angular distributions in Xe + Sn at E/A=49 MeV [14]. The distribution of the out-of-plane emission is taken as: $P(\sin\phi) = A \exp(-\omega^2 \sin^2\phi)$ where ϕ is the out-of-plane angle, ω represents the width of the distribution, and A is a normalization constant. The model predictions have been filtered by the detector acceptance and compared to the experimentally measured angular distributions presented in Fig. 1. Comparison of the measured and predicted distributions for different values of ω indicates that the magnitude of ω is ≈ 0.5 . Within the framework of a fissioning nucleus, the parameter ω can be related to angular momentum [19]: $J^2 = \frac{2\omega^2 I_{eff} T}{\hbar^2}$ where T is the temperature and I_{eff} is the moment of inertia, calculated as: $I_{eff} = \frac{2}{5} M R^2 F_I$. The mass, M, is approximated as: $M = m_0 c^2 A_{PLF^*}$ where $m_0 c^2$ is the rest mass of the nucleon and $A_{PLF^*} = \left(\frac{N}{Z}\right)_{projectile} Z_{PLF^*}$. The effective radius of the dinuclear configuration is given by $R^2 F_I$ with $R = r_0 A^{1/3}$ and the deviation from a sphere accounted for by F_I [20]. The value of the radius constant r_0 is taken as 1.2 fm. As F_I has not been calculated for a system as light as the PLF* under consideration, we use the published value for the significantly heavier nucleus ^{149}Tb [20]. Assuming a temperature of T=3-5 MeV for the system undergoing binary decay, we calculate an an-

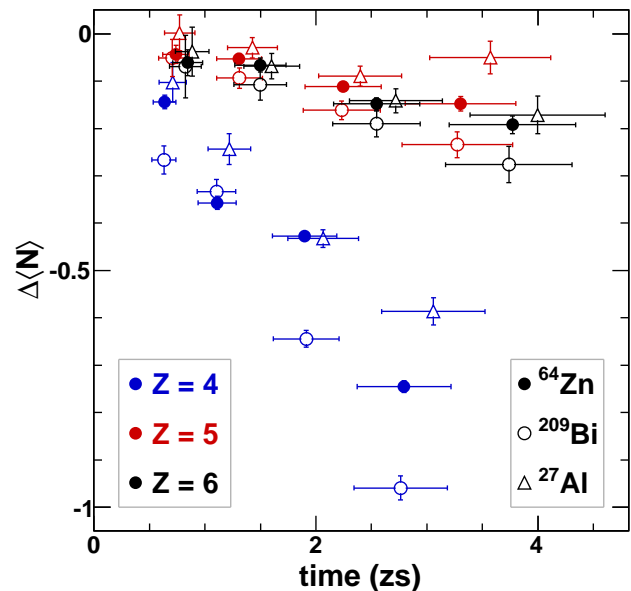


FIG. 4: (Color online) Dependence of the average differential neutron number on time for $Z_L = 4, 5$ and 6 for the reactions $^{64}\text{Zn} + ^{64}\text{Zn}$, ^{209}Bi and ^{27}Al . (See text for details)

gular momentum $J=6\pm 1 \hbar$. The rotation time is thus given by: $t = \frac{\alpha I_{eff}}{J\hbar}$. The deduced timescale is shown in Fig. 3. It should be noted that the timescale deduced ($t \leq 3$ zs) is consistent with previously published results [10, 21, 22]. For reference, the angular velocity calculated for this light dinuclear complex is $0.4\text{-}0.5 \times 10^{21}$ rad/sec.

Having associated the rotation angle with a timescale, it is now possible to observe two timescales evident in Fig. 3. The first observation is that for this system even for times as long as 3 zs, i.e. 900 fm/c, the $\langle N \rangle$ of the Z_L fragment is still changing indicating that N/Z equilibration is a slow process. In addition, operating on a faster timescale of ≈ 1 zs, the v_{REL} dependence observed for the most backward angles is overpowered by the Coulomb effect that characterizes forward emission [23]. The pattern observed for $Z_L=4$ in Fig. 3 indicates that even for backward angles a correlation exists between the rotation angle dependence and the v_{REL} dependence for $\langle N \rangle$. However, disentangling the intrinsic N/Z gradient from the Coulomb contribution at backward angles requires knowledge of the detailed configuration of the dinuclear system. This disentanglement is beyond the scope of the present work. We therefore examine the dependence of $\langle N \rangle$ on time, integrated over v_{REL} .

Shown in Fig. 4 is the time dependence of $\langle N \rangle$ for $Z_L=4, 5$, and 6 fragments. To compare the change in $\langle N \rangle$ for different targets and different Z_L fragments, we subtracted the extrapolated value of $\langle N \rangle$ at $t=0$. This extrapolated value was determined by performing a linear fit of $\langle N \rangle$ versus time. It is interesting that the data shown in Fig. 4 clearly fall into two groups. While $Z_L=4$ exhibits a strong dependence of $\Delta\langle N \rangle$ on time, $Z_L=5$ and 6 fragments manifest a much weaker dependence. In the

case of $Z_L=4$ fragments, a strong and clear target dependence is evident. Close examination of the data for $Z_L=5$ and 6 fragments reveals that the same target dependence exists though it is smaller in magnitude. For $Z_L = 4$, the Bi target is associated with the largest change in $\langle N \rangle$, ≈ 1 . The Zn and Al targets exhibit smaller changes of 0.75 and 0.6 respectively. The horizontal error bars shown in the figure are primarily governed by an estimated uncertainty of $\Delta J=1\hbar$. It should be noted that the magnitude of the change in $\langle N \rangle$ is considerably larger than that previously reported for the Xe + Sn system [10].

For Be fragments the large slope of $\Delta\langle N \rangle$ versus time indicates significant equilibration occurs on the timescale of 3 zs. One can imagine that the rate of equilibration is governed by the initial difference in N/Z between the Z_L and Z_H fragments, i.e. a gradient in N/Z within the PLF*. Confirming this perspective is the behavior of Be fragments for different targets. The data for the Bi target manifests the largest slope and the one for the Al target the smallest slope corresponding directly to the neutron-enrichment of the Z_L fragment as evident in Fig. 2. This target dependence suggests a fundamental result. The neutrons transferred from the target do *not* equilibrate within the PLF* prior to it attaining the dinuclear configuration. If they did, all three targets would manifest the same equilibration rate. Thus the experimental data directly indicate that the equilibration rate of $\langle N \rangle$ is governed by the initial N/Z gradient in the dinuclear system.

It is reasonable to imagine that the initial difference in N/Z between the Z_L and Z_H fragment is not the only factor influencing the equilibration process. As N/Z equilibration involves nucleon transfer between the Z_L and Z_H fragments, a “window” between the two fragments must exist. The cross-sectional area of this window and its lifetime impacts the net transfer of nucleons and hence the rate and degree of equilibration [24]. One might expect that the configurations for Be, B, and C fragments are not identical. Earlier work [14] concluded from the angular distribution of Z_L fragments that smaller Z_L fragments such as Be were associated with long, skinny necks. In contrast, larger Z_L fragments such as C or O fragments were associated with shorter, thicker necks. Configurations with small cross-section “windows” would impede the equilibration process. Thus, the rate of equilibration observed represents the competition between the differ-

ence in initial N/Z of the Z_L and Z_H fragments and the evolving configuration of the dinuclear complex.

In summary, to investigate the N/Z equilibration timescale for a dinuclear complex, we have focused on the binary decay of a PLF*. For this system, we have shown that the isotopic composition ($\langle N \rangle/Z$) of the fragments depends on the rotation angle of the dinuclear complex. Moreover, the N/Z of the Z_L fragment depends on the neutron-richness of the target. While we observe these effects for $Z_L=4, 5$, and 6 fragments, they are strongest in the case of Be fragments. This large magnitude for Be fragments can be qualitatively understood as due to the absence of ^8Be in the isotopic distribution making Be a sensitive probe of the equilibration process. Within our analysis, the N/Z equilibration is related to the change in average neutron number, $\Delta\langle N \rangle$, experienced by the Z_L fragment. Using the rotation angle of the dinuclear complex we deduce the timescale on which the N/Z equilibration occurs. The equilibration persists for as long as 3-4 zs. The equilibration rate is large for Be fragments as compared to B and C fragments which manifest a comparable rate. Clear evidence for a target dependence of the equilibration rate is observed in the case of Be fragments. The largest equilibration rate (Bi target) is associated with the largest initial neutron-enrichment of the Z_L fragment. These differences in equilibration rate can be related to different initial N/Z gradients within the dinuclear configuration for the different targets. While qualitatively the physical picture associated with these observations is clear, a more detailed understanding of the N/Z equilibration will require comparison with a theoretical model that describes nucleon transport within the dinuclear complex.

Acknowledgments

This work was supported by the U.S. Department of Energy under Grant Nos. DEFG02-88ER-40404 (IU) and DE-FG03-93ER40773 (TAMU). Support from the Robert A. Welch Foundation through Grant No. A-1266 is gratefully acknowledged. Collaboration members from Université Laval recognize the support of the Natural Sciences and Engineering Research Council of Canada.

-
- [1] J. Lattimer and M. Prakash, *Astrophys. J.* **550**, 426 (2001).
 - [2] A. Steiner et al., *Phys. Rep.* **411**, 325 (2005).
 - [3] H. T. Janka et al., *Phys. Rep.* **442**, 38 (2007).
 - [4] P. Möller et al., *Phys. Rev. Lett.* **108**, 052501 (2012).
 - [5] M. B. Tsang et al., *Phys. Rev. C* **86**, 015803 (2012).
 - [6] M. B. Tsang et al., *Phys. Rev. Lett.* **92**, 062701 (2004).
 - [7] A. L. Keksis et al., *Phys. Rev. C* **81**, 054602 (2010).
 - [8] Z. Kohley et al., *Phys. Rev. C* **86**, 044605 (2012).
 - [9] E. D. Filippo et al., *Phys. Rev. C* **86**, 014610 (2012).
 - [10] S. Hudan et al., *Phys. Rev. C* **86**, 021603(R) (2012).
 - [11] D. Thériault et al., *Phys. Rev. C* **74**, 051602 (R) (2006).
 - [12] T. Paduszynski et al., *Nucl. Instr. and Meth. A* **547**, 464 (2005).
 - [13] B. Davin et al., *Phys. Rev. C* **65**, 064614 (2002).
 - [14] A. B. McIntosh et al., *Phys. Rev. C* **81**, 034603 (2010).
 - [15] P. Glässel et al., *Z. Phys. A* **310**, 189 (1983).
 - [16] J. Lecolley et al., *Phys. Lett. B* **354**, 202 (1995).
 - [17] V. Baran et al., *Phys. Rev. C* **85**, 054611 (2012).
 - [18] J. Colin et al., *Phys. Rev. C* **67**, 064603 (2003).

- [19] R. Vandenbosch and J. R. Huizenga, *Nuclear Fission* (Academic Press, 1973).
- [20] N. Carjan and M. Kaplan, Phys. Rev. C **45**, 2185 (1992).
- [21] G. Casini et al., Phys. Rev. Lett. **71**, 2567 (1993).
- [22] S. Piantelli et al., Phys. Rev. Lett. **88**, 052701 (2002).
- [23] S. Hudan et al., Phys. Rev. C **71**, 054604 (2005).
- [24] W. J. Swiatecki, Physica Scripta **24**, 113 (1981).